

# Solubilizing Carbon Nanotubes through Noncovalent Functionalization. Insight from the Reversible Wrapping of Alginic Acid around a Single-Walled Carbon Nanotube

Yingzhe Liu,<sup>†</sup> Christophe Chipot,<sup>‡,§</sup> Xueguang Shao,<sup>†</sup> and Wensheng Cai<sup>\*,†</sup>

College of Chemistry, Nankai University, Tianjin, 300071, P.R. China, and Theoretical and Computational Biophysics Group, Beckman Institute, University of Illinois at Urbana–Champaign, Urbana, Illinois 61801

Received: November 21, 2009; Revised Manuscript Received: January 24, 2010

Carbon nanotubes coated with alginic acid (AA) through noncovalent functionalization have been shown to be soluble and dispersed in water. In the present contribution, all-atom molecular dynamics simulations have been performed to probe the self-assembly mechanism that underlies the formation of complexes by AA and a single-walled carbon nanotube (SWCNT), both in the gas phase and in an aqueous solution. Results of these simulations reveal that AA can wrap around SWCNT by virtue of van der Waals attractions and organize into a compact helical structure, a process induced in the gas phase by hydrogen-bonding interactions. In contrast, in an alginate aqueous solution, a loose helical wrapping mode is found to be favored by virtue of electrostatic repulsions in conjunction with the weakening of hydrogen-bonding interactions. Documented experimentally (Liu, Y.; et al. *Small* 2006, 2, 874–878) and coined “Great Wall of China” motif, the typical arrangement of AA residues around the tubular structure, conducive to dissolve nanotubes, is observed in the present simulations. Investigation of metal cations binding to AA suggests that calcium ions can mediate aggregation of AA chains by interacting strongly with the carboxylate groups, thereby leading to reverse unwrapping. The results reported in this work shed meaningful light on the potential of noncovalent functionalization for solubilizing carbon nanotubes, and open exciting perspectives for the design of new wrapping agents that are envisioned to form the basis of innovative nanomaterials targeted at chemical and biomedical applications.

## 1. Introduction

Carbon nanotubes (CNTs) have been the object of an increased interest on account of their remarkable structural, mechanical, and electrical properties,<sup>1</sup> offering broad potential applications that range from nanodevices,<sup>2</sup> gas storage,<sup>3</sup> nanoelectronics,<sup>4</sup> to drug delivery.<sup>5</sup> Advancement in these research areas has, however, been severely impeded as a result of the inherently poor solubility of CNTs in aqueous and organic solvents. Functionalization, which is normally classified as covalent modification<sup>6</sup> and noncovalent decoration,<sup>7</sup> has been applied to overcome this shortcoming. However, the former route partially damages the intrinsic structural and electrical properties of pristine nanotubes. In contrast, the latter route can potentially preserve the  $\pi$ -conjugated system by means of wrapping or encapsulating polymers, as well as adsorption of small molecules. This strategy has, therefore, been widely employed, in particular by combining biomolecules as a function of their biocompatibility.<sup>8</sup>

In recent years, immense progress has been made in experiments delving into the intriguing topic of noncovalent coupling. Several research groups have found that natural biomolecules, including amylose,<sup>9,10</sup> cyclodextrin,<sup>11–13</sup> peptides,<sup>14</sup> proteins,<sup>15</sup> and DNA<sup>16,17</sup> can eventually achieve the goal of nanotube solubilization and dispersion. For example, Stoddart et al.<sup>9</sup> showed that the left-handed helix amylose previously self-

assembled with iodine molecules could wrap single-walled carbon nanotubes (SWCNTs) to form soluble complexes. Subsequently, it was proven by Kim<sup>10</sup> that the helical state of amylose is not a prerequisite for amylose encapsulation of CNTs. In particular, Zheng et al.<sup>16</sup> have reported their experimental observations of a single-stranded DNA helix surrounding the tubular surface via  $\pi$ - $\pi$  stacking, which constitutes an effective route for dispersing CNTs in water. In addition, these nanomaterials possessing different electronic structures can be separated by ion-exchange chromatography.<sup>17</sup>

Along with experimental investigations, theoretical studies, in particular molecular dynamics (MD) simulations, have been endeavored to decipher the mechanism through which biomolecules and nanotubes interact. Among these studies, a noteworthy emphasis was put on noncovalent functionalization with DNA.<sup>18–22</sup> The study of Gao et al.<sup>18</sup> revealed, for instance, that DNA octamers could be spontaneously inserted into, or adsorbed onto SWCNTs, depending on the size of the tubular cavity in the aqueous environment. Encapsulation is subsequently detected experimentally by means of fluorescence microscopy.<sup>23</sup> Klein and co-workers<sup>19</sup> studied in a systematic fashion the self-assembly mechanisms, structure, and energetic properties of nanomaterials and found that helical wrapping results from the balance of electrostatic and torsional interactions within the sugar–phosphate. The free-energy landscape of this system was subsequently explored using replica-exchange molecular dynamics (REMD) simulations which has proven to be particularly suited for extensive conformational sampling.<sup>20,21</sup> In addition to DNA, the interaction of amylose<sup>24</sup> and polymer<sup>25</sup> with nanotubes was also discussed.

\* To whom correspondence should be addressed. E-mail: wsc@nankai.edu.cn.

<sup>†</sup> Nankai University.

<sup>‡</sup> University of Illinois at Urbana–Champaign.

<sup>§</sup> On leave from Équipe de Dynamique des Assemblages Membranaires, UMR 7565, Nancy Université, BP 239, 54506 Vandœuvre-lès-nancy Cedex, France.

Recently, Liu et al.<sup>26</sup> reported that alginic acid (AA), a natural polysaccharide harvested from brown algae, can solubilize and disperse efficiently multiwalled carbon nanotubes (MWCNTs) in water, because of a unique arrangement of AA, reminiscent of the Great Wall of China architecture. It was suggested on the basis of <sup>1</sup>H NMR spectra that two  $\beta$ -D-mannuronic acid units of the M segment can lie on the surface of the MWCNTs and one of the two  $\alpha$ -L-guluronic acid units of the G segment can be oriented perpendicular to that surface. Another exciting phenomenon was also found by adding alkaline-earth-metal cations to the AA–MWCNT complexes, which results in the precipitation of MWCNTs in the aqueous solution. AA is widely used in the food and pharmaceutical industries due to its recognized lack of toxicity.<sup>27</sup> Reversible association, therefore, has extensive potential applications in aqueous biological systems and medicinal chemistry. However, it ought to be stressed that AA–MWCNT solutions are very stable toward disruption by alkaline-metal cations. Moreover, many aspects of the interactions at play remain poorly understood owing to the lack of atomic-level information.

In the present work, the AA–SWCNT system is investigated by means of all-atom MD simulations, both in the gas phase and in water, to explore the mechanism whereby self-assembly proceeds and the structural properties of the complex. The influence of the sizes of the nanotube on the morphology of the complex is taken into account. In addition, the mechanism whereby  $\text{Ca}^{2+}$  and AA interact is examined to explain why reverse unwrapping can occur.

## 2. Methods

### 2.1. Molecular Models.

AA is an unbranched binary copolymer, consisting of (1,4)-linked  $\beta$ -D-mannuronic acid (M) and  $\alpha$ -L-guluronic acid (G). The M/G ratio drastically affects certain properties of alginate, such as its structure, biocompatibility, transmittancy, and viscoelasticity. Here, a simple structural motif of AA embracing repetitive blocks of consecutive GGMM residues is investigated (see the Supporting Information). The initial coordinates of the G and M monomers were built based on available crystal structures (1Y3P) in the Protein Data Bank. The structures were optimized using a conjugate-gradient energy-minimization algorithm. The AA chain was constructed by periodically (1,4)-linking two adjacent monomers together according to the sequence. On account of the insolubility of AA, sodium alginate was used in explicit water. Sodium ions were added to neutralize exactly the deprotonated carboxylic acid groups.

In practice, carbon nanotubes generally contain defects found on the outer surface, and/or functional groups located at their edges. To simplify the molecular systems, undecorated and ideal SWCNTs were modeled. It has been suggested that, among chiral and nonchiral structures, armchair SWCNTs possess the strongest adhesion properties with polymers.<sup>28</sup> Accordingly, five sizes of SWCNTs, viz., (8,8), (12,12), (16,16), (20,20), and (24,24), were constructed. The parameters of  $\text{sp}^2$  carbon atoms devoid of a net atomic charge were used to describe the SWCNTs. The nanotubes were frozen in all of the simulations with the participating C–C bonds constrained to their equilibrium length of 1.42 Å. The SWCNTs of pseudoinfinite length employed in the aqueous medium were built by repeating the cell along the longitudinal axis of the nanotube using periodic boundary conditions (PBCs). The detailed consideration in building a pseudoinfinitely long SWCNT as well as a general description of the molecular systems considered in this study can be found in the Supporting Information.

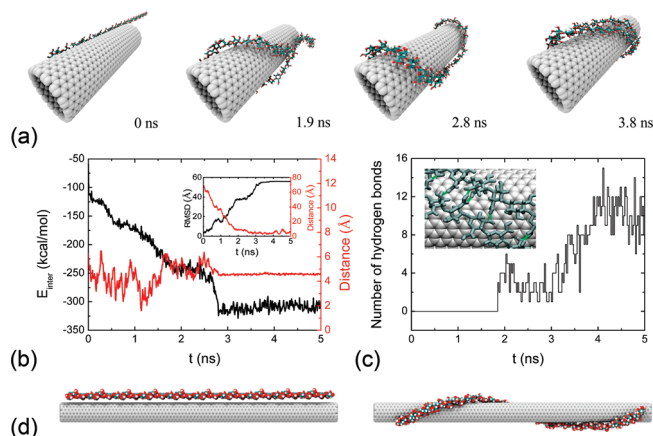


**Figure 1.** (a) Wrapping process retrieved from the simulation of the AA–SWCNT system. AA: (GGMM)<sub>10</sub> with length of ca. 190 Å. SWCNT: (16,16) with length of 72.56 Å. (b) Time evolution of the interaction energy (black) and the average vertical distance (red) between the centroid of each residue and the tubular surface. Inset: The distance root-mean-square deviation (rmsd) over the heavy atoms of the AA chain with respect to the initial structure (black) and the center of mass (COM) distance (red) between AA and SWCNT as a function of time. (c) Number of hydrogen bonds formed between the neighboring helical turns of AA as a function of time. The hydrogen-bonding criterion here is the angle  $\text{O}\cdots\text{H}\cdots\text{O} > 150^\circ$  and the distance  $\text{O}\cdots\text{O} < 3.5$  Å. Inset: Snapshot of the complex. Hydrogen bonds are highlighted in green. (d) Left: Initial arrangement of the (8,8) SWCNT with a length of about 198 Å and a 40-residue AA chain. Right: A snapshot obtained from the 70 ns MD trajectory.

### 2.2. Molecular Dynamics Simulations.

All simulations were performed with the MD program NAMD2.6.<sup>29</sup> The specific CSFF force field<sup>30</sup> for carbohydrate solution simulations and the TIP3P<sup>31</sup> water model were used to describe the molecular assembly. The simulations in the gas phase were carried out at 300 K. In the aqueous solution, the isobaric–isothermal ensemble was employed with PBCs. The temperature and the pressure were maintained at 300 K and 1 bar, respectively, employing Langevin dynamics and the Langevin piston method.<sup>32</sup> Long-range electrostatic forces were taken into account by means of the particle-mesh Ewald (PME) approach.<sup>33</sup> van der Waals interactions were truncated smoothly with a spherical cutoff of 12.0 Å radius. The equations of motion were integrated in vacuo with a time step of 0.5 fs, and of 2.0 fs in the aqueous solution, employing the multiple time step Verlet r-RESPA algorithm.<sup>34</sup> Covalent bonds involving hydrogen atoms were constrained to their equilibrium value by means of the SHAKE/RATTLE algorithms.<sup>35,36</sup> Analysis and visualization of MD trajectories were performed with VMD.<sup>37</sup>

## 3. Results and Discussion

### 3.1. Wrapping in Vacuo.

To probe the binding affinity of CNT and AA in the gas phase, a simulation was performed, in which a 40-residue AA chain was placed in the vicinity of the (16,16) SWCNT surface within the cutoff distance for van der Waals interactions. Figure 1a shows a selection of snapshots obtained from the MD trajectories, representing key events in the process of spontaneous assembly. Initially, the AA chain is parallel to the longitudinal axis of the nanotube. It then moves toward the outer surface of the SWCNT as a result of attractive van der Waals interactions, crawls onto the tubular structure, and gradually wraps it. After 1.9 ns, owing to favorable hydrogen-bonding interactions, the AA chain curls into a ring pattern toward the head of the nanotube, while the tail of the chain is still rather disordered. Driven by van der Waals

attractions, the tail of the AA chain also wraps around the nanotube after 2.8 ns. As new hydrogen bonds form progressively, a perfect helical structure is completely formed after 3.8 ns. The analysis of the 5 ns MD trajectory is displayed in Figure 1b. The sharp decrease of the interaction energy at about 2.8 ns corresponds to the close contact of the whole AA chain to the surface of the SWCNT.

During the wrapping process, hydrogen-bonding interactions appear to play a significant role on the final conformation. Modification of the hydrogen-bond network was monitored in the course of the formation of the helix (see Figure 1c). Only those hydrogen bonds formed between adjacent turns were counted, excluding those existing in each residue and between neighboring ones. It is apparent from the figure that no hydrogen bonds were created in the early stage of the simulation. The increase observed after 2 ns indicates that the first turn of the helix is steady. On account of the hydrogen-bonding interactions, self-organization of the first turn and the remainder of the chain are witnessed, resulting in an orderly spiral structure at the final stage of the simulation. The large number of hydrogen bonds formed after 4 ns is suggestive that a compact helical structure has been obtained. From the above discussion, it can be inferred that van der Waals attraction constitutes the leading driving force responsible for the wrapping of AA around the SWCNT, and hydrogen-bonding interactions are a key element in the formation of the compact spiral.

Another AA–SWCNT model, in which SWCNT is slightly longer than AA (see Figure 1d, left), was also simulated. The resulting 70 ns MD trajectory reveals that AA can wrap smoothly around the SWCNT with a long-pitch helical structure (see Figure 1d, right). Due to the lack of strong hydrogen-bonding interactions within adjacent turns, the AA conformation appears to be more flexible than the compact helical structure. Further analysis of the energies for the two representative wrapping modes obtained in our simulations (see the Supporting Information) indicates that the compact one is energetically favored compared to the loose helical structure. This is because additional hydrogen bonds can compensate for the increasing strain arising from the tight helical turns. In the case of the long tubular structure, formation of a loose helix has, however, been observed reproducibly on the basis of repeated simulations, whereas the compact helical wrapping did not occur. This can be explained by the existence of pronounced energy barriers, probably insurmountable over the time scale explored.

In addition to the helical organization, disordered adsorptions of AA on the surface of the SWCNT were also observed in several simulations run concomitantly. This result is not unexpected, given that AA is a flexible polymer possessing many degrees of freedom, hence corresponding to a rugged potential energy landscape featuring many local minima. Conformational sampling is necessarily incomplete over a few tens of nanoseconds. Furthermore, the final configurations obtained within the time scale amenable to MD simulations strongly depend upon the initial conditions of the molecular system, such as the initial conformation of AA and the position of the latter relative to the SWCNT. Therefore, whether or not the compact wrapping mode constitutes the global minimum of the free-energy landscape still remains to be determined. To clarify this issue, exhaustive sampling of the latter free-energy landscape would be needed,<sup>20,21</sup> which evidently goes beyond the scope of the present study.

To examine the influence of the diameter of the nanotube on the ordering and the compactness of the wrapping, a number of arbitrary decisions have to be made. A turn of the AA chain

is initially aligned along the longitudinal axis of the nanotube (Figure 2a) to overcome possible high-energy barriers. Five types of nanotubes, viz., the (8,8), (12,12), (16,16), (20,20), and (24,24) SWCNTs, were considered. In each molecular system, the initial position and conformation of the AA fragment were identical. A 5 ns MD simulation was carried out for each one of the five systems.

As can be seen in Figure 2b, all of the wrapping processes reach a well-equilibrated state more rapidly than in the case of the linear AA–SWCNT system. Analysis of the morphology of the AA chain (see the Supporting Information) shows that, at variance with the (16,16), (20,20), and (24,24) SWCNTs, perfect helices cannot form around the (8,8) and (12,12) nanotubes. The snapshots of the configurations of the five complexes after 5 ns are shown in Figure 2c and d. The AA chain is found to form an ordered helical structure around the (16,16), (20,20), and (24,24) SWCNTs, whereas, for the (8,8) and (12,12) SWCNTs, the conformation of the AA chain is a partial helical structure with a “tail” lying on the surface of the nanotube. This may be explained by the relative high rigidity of the AA chain, which mainly stems from the <sup>1</sup>C<sub>4</sub> conformation of the G residues (see the Supporting Information). The rigidity of AA increases the strain in each turn of the helix. It is, therefore, reasonable to hypothesize that, in vacuo, it is difficult for AA to form a compact helical structure around a narrow nanotube. The critical size in the present simulations is (16,16). On the other hand, enlarging the turn of the helix can release some strain for a given nanotube. This may result in a general trend toward tilting the helix with narrower nanotubes, as can be seen in the structures depicted in Figure 2d.

In addition, a loose helical wrapping mode was also considered with five nanotubes of distinct diameter. In all five systems, the AA chain was found to wrap around the SWCNT smoothly, although both ends appear to be less tightly drawn. The morphology of the AA chain is obviously not affected by the diameter.

**3.2. Wrapping in an Aqueous Solution.** To probe whether the compact helical structures favored by the gas phase still exist in the aqueous solution, additional 30 ns MD simulations were performed in the latter environment for the five equilibrated structures described previously. Considering the low solubility of AA in water, alginate was modeled in the simulations by ionizing the carboxylic acid groups. Analysis of the 30 ns MD trajectories for the five molecular systems is suggestive of a tendency exhibited by AA to unwrap from the nanotubes. The evolution of the distance separating the chain from the surface of the nanotube was calculated, as delineated in Figure 3. It is apparent that AA moves gradually away from the SWCNT in the five molecular assemblies. This result can be ascribed to an electrostatic repulsion and the significant weakening of the hydrogen bonds formed between neighboring turns, which is a consequence of the deprotonation of the carboxylic acid moieties, as well as an effect of the solvent. In addition, the balance between hydrogen-bonding interactions and the structural strain established in the gas phase was in large measure destroyed in the aqueous solution. Some of the strain caused by the exaggerated bending of the rigid AA chain was relieved by the unwrapping process.

To explore the stability of the loose wrapping mode in the aqueous media, the initial model, identical to that in Figure 1d (left), was hydrated by 29 578 water molecules. Up to 30 ns of MD trajectory were then generated. A long-pitch helical structure formed with the tail of AA merely adsorbed on the surface (see Figure 4a). Analysis of the trajectory shows that

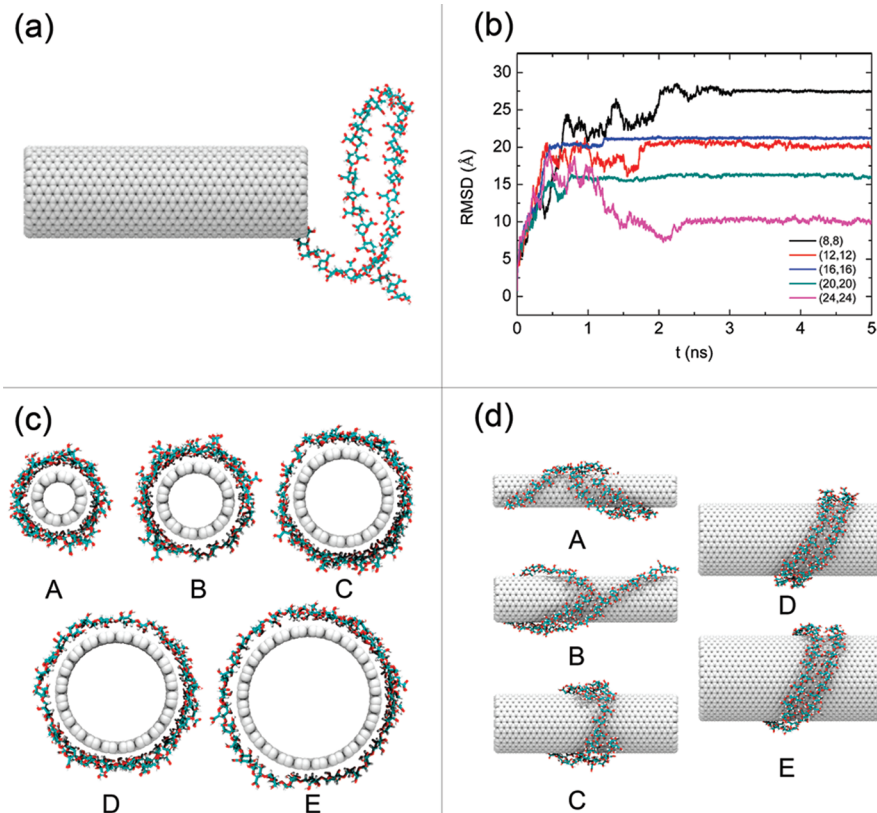


**Figure 2.** (a) The initial structure of a (16,16) SWCNT with a length of ca. 72 Å and a 40-residue long AA fragment. (b) Time evolution of the distance rmsd over the heavy atoms of AA with respect to their initial positions. (c and d) Equilibrium structure of the complex after 5 ns from different viewpoints. Structures A–E represent the complex of AA and the (8,8), (12,12), (16,16), (20,20), and (24,24) SWCNT, respectively.

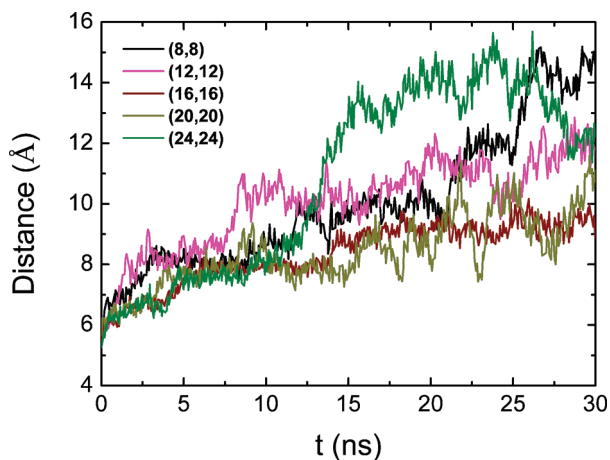


**Figure 3.** Average vertical distance separating the centroid of the AA residues and the tubular surface in the radial direction, as a function of time.

this loose wrapping mode involves stronger interactions with the SWCNT (see Figure 4b), which is at variance with the complex investigated in the gas phase. Furthermore, the loose structure can reduce effectively the electrostatic repulsion between neighboring carboxylate groups (Figure 4c). The loose helical wrapping mode, therefore, appears to be particularly robust in solution, whereas the compact form only corresponds to a metastable state of the complex.

As a basis of comparison, the amylose–SWCNT system was simulated in an aqueous solution for 26 ns. A 24- $\alpha$ -D-glucose-residue amylose fragment and a narrow nanotube, (6,6) SWCNT, were selected as a representative molecular assay for this simulation. The preconstructed helical structure was found to

be more compact over the entire MD simulations, with the formation of hydrogen bonds. The average vertical distance separating the centroids of the glucose units from the surface of the nanotube is only 4.25 Å, and the average number of hydrogen bonds formed between neighboring turns of the helix is 5, thus, suggesting that the nanotube was covered tightly. It is commonly known that the amylose chain is very flexible as a result of its unique structural features. It can, therefore, adapt itself to carbon nanotubes of different diameters, and even wrap around narrow SWCNTs. Furthermore, spontaneous wrapping of amylose from a straight conformation onto a (8,8) SWCNT was also simulated in the water phase. As expected, a perfect helical wrapping was monitored within a few nanoseconds. Although no hydrogen bonds were found to be formed between neighboring turns, leading to an increase in the helix pitch, the helical structure was still found to be more compact than in the case of AA. The surface coverage of AA on the SWCNT is lower than that with amylose, in good agreement with experiment.<sup>9,26</sup> This means that fewer AA can solvate the nanotubes. Figures depicting the complexes and analysis of the trajectories are provided in the Supporting Information.

**3.3. “Great Wall of China” Structural Arrangement.** To rationalize the preference for this particular arrangement, statistical analysis of the 10 ns simulation that brought to light a multiturn helical alginate chain wrapped around the SWCNT was carried out. The initial molecular model consisting of a 160-residue AA helix wrapped around a (20,20) SWCNT of length equal to ca. 198 Å was constructed by hand (see the Supporting Information). In addition, an analysis of the trajectory for the loose wrapping mode depicted in Figure 4a was performed.

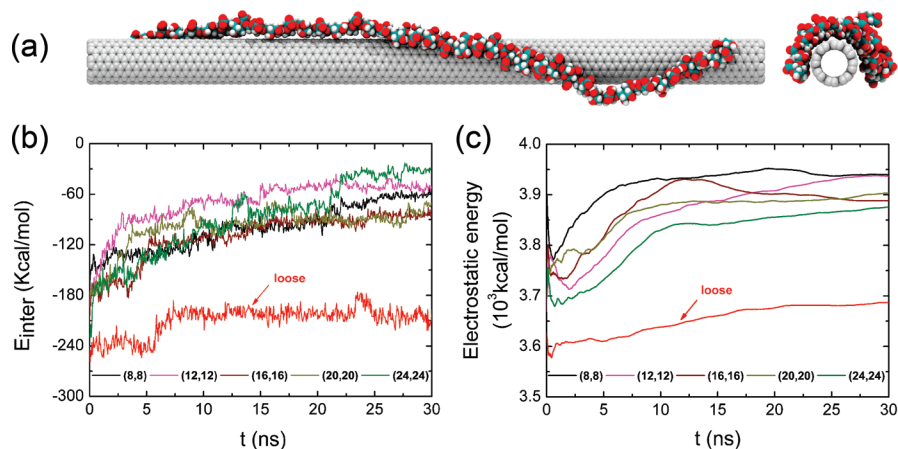


**Figure 4.** (a) Snapshot of the complex obtained from the 30 ns trajectory, excluding water and ions for clarity. A loose helical wrapping is observed. (b) Interaction energy of the 40-residue AA and six distinct SWCNTs. (c) Time evolution of the average electrostatic energy for the AA chains in the six systems.

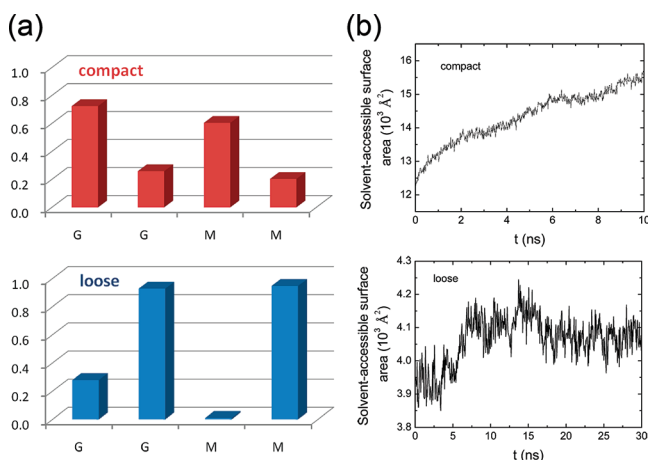


**Figure 5.** (a) Distribution of angle  $\alpha$  between 0 and  $75^\circ$  for every residue in the GGMM sequence. (b) Hydrophilic solvent-accessible surface area of AA. Here, hydroxyl and carboxylate groups are taken into account.

Here, the orientation of a residue is defined by the angle,  $\alpha$  (see the Supporting Information), formed by the radial vector and the bisector of the carboxylate moiety. Smaller angles are indicative of carboxylate groups lying far away from the nanotubes, whereas larger angles correspond to an orientation in which the latter functional groups face the hydrophobic surface of the nanotubes. The probability to find  $\alpha$  ranging between 0 and  $75^\circ$  for each residue of the GGMM sequence (see Figure 5a) reveals that the carboxylate group of every other residue exhibits a marked tendency to be exposed to the solvent rather than to approach the surface of the tubular structure. Interestingly enough, the loose wrapping mode yields similar results. This is somewhat at variance with experimental observations, mainly because the chosen GGMM sequence cannot embrace the variety of structural features characteristic of a common AA chain with complicated arrangements. The preferred orientations, nevertheless, still correspond to a “Great Wall of China”-like pattern.<sup>26</sup>

It is reasonable to believe that hydrophobic interactions are responsible for the observed preferred orientations, which is manifested in the increasing hydrophilic solvent-accessible surface areas of AA as a function of time (see Figure 5b). In turn, this preference stems from favorable hydrophobic interactions, which greatly help dissolve SWCNT-AA complexes in water.

### 3.4. Unwrapping Process Controlled by Calcium Ions. It

has been reported that addition of alkaline-earth metal such as calcium ions to the solution of AA-wrapped MWCNTs resulted in the precipitation of the nanotubes in the aqueous solution.<sup>26</sup> In sharp contrast, AA-MWCNT complexes are found to be remarkably stable for months in the presence of sodium ions.<sup>26</sup> To apprehend the role played by metal ions, the interaction mode of the latter with poly-GGMM chains was investigated. Previous studies have revealed that  $\text{Ca}^{2+}$  can interact with long stretches of pure G blocks following the well-known egg-box pattern,<sup>38</sup> and this unusual interaction mode is responsible for the formation of gels. The model assumes that two pairs of two consecutive G residues pertaining to different chains can form a cavity susceptible to accommodate one  $\text{Ca}^{2+}$  ion due to its  ${}^1\text{C}_4$  conformation. Hence, two G-rich alginate chains adopting a characteristic zigzag shape can associate through the coordination of  $\text{Ca}^{2+}$  ions. Experimental and theoretical studies<sup>39–42</sup> also reveal that G residues exhibit a high specificity for  $\text{Ca}^{2+}$  binding and that  $\text{Ca}^{2+}$  ions adopt distinctive positions in well-adapted cavities. In sharp contrast, M residues do not exhibit any stereospecificity for  $\text{Ca}^{2+}$  binding. In addition, a recent investigation<sup>43</sup> has brought to light the binding affinity of  $\text{Ca}^{2+}$  toward MG alternating sequences.

In the present work, the egg-box model was considered initially for the sequences of GGMM (see the Supporting Information). The results of the simulations, however, reveal that the cavities formed by the G residues cannot hold steadily the prelocated  $\text{Ca}^{2+}$  ions. This may be ascribed to the length of consecutive G blocks, excessively short to preserve the rigidity of the cavities. As can be seen from the MD trajectory,  $\text{Ca}^{2+}$  ions exhibit a high affinity toward carboxylate groups. On the basis of this observation, an alternative binding model was proposed (see the Supporting Information). In an initial model, two 16-residue zigzag-shaped chains were aligned parallel to each other, and eight ions were placed in the gap formed by neighboring carboxylate groups belonging to different fragments. Additional ions were inserted randomly to enforce electric neutrality of the system. A 10 ns simulation of the two chains in the presence of  $\text{Ca}^{2+}$  ions was then performed to delve into the interaction mechanism. Furthermore, a separate simulation was also carried out with monovalent sodium ions as a contradistinction.

As can be clearly seen in Figure 6a, the  $\text{Ca}^{2+}$  ions cooperate in an orderly fashion with every other residue through favorable electrostatic interactions. In particular, one  $\text{Ca}^{2+}$  ion is found

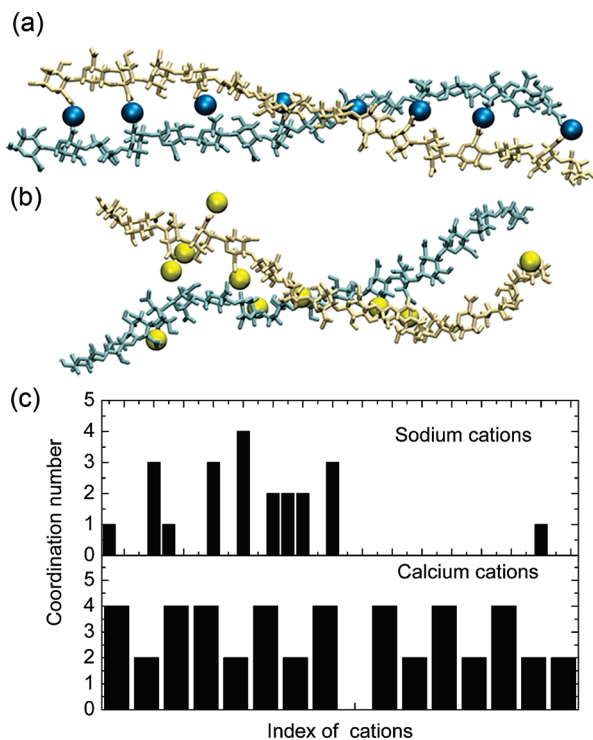


**Figure 6.** Two snapshots of AA chain binding with (a) Ca<sup>2+</sup> and (b) Na<sup>+</sup> ions. Other particles are not shown for clarity. (c) The average coordination number of every Ca<sup>2+</sup> and Na<sup>+</sup> ion. Only the oxygen atoms of the carboxylate groups found within 5 Å from the participating ions were taken into account.

to coordinate to four carboxylate oxygen atoms. Two chains linked by calcium cations prefer to form a stable double helical structure to enhance van der Waals interactions. It is reasonable to expect that many chains could aggregate into bundles in the presence of large counts of Ca<sup>2+</sup> cations, in line with the characteristic zigzag structure. On the contrary, the interaction of Na<sup>+</sup> with AA was found to be very weak, to the extent that the monovalent cation could hardly link the two chains together (see Figure 6b). An energy analysis is supplied in the Supporting Information. The average coordination number of each cation was estimated over the entire MD simulations, as delineated in Figure 6c. On the basis of this analysis, a possible zipper-like binding mode is proposed for Ca<sup>2+</sup> with AA of poly-GGMM sequence.

In addition, considering the difficulty of simulating at the atomic level the unwrapping process of the AA chain from the perfectly wrapped AA–SWCNT complex, an alternative approach was investigated to probe the competitive binding of Ca<sup>2+</sup> to AA and SWCNT. This route was explored by applying an external force to pull one AA chain out of the AA dimer linked by Ca<sup>2+</sup> ions and the AA–SWCNT complex, respectively, and comparing the corresponding free-energy profiles that characterize the pulling processes. The latter were probed employing steered molecular dynamics (SMD)<sup>44</sup> simulations, as implemented in the NAMD software.<sup>29</sup> The external force was applied on one linked oxygen atom located in the middle of the AA chain. The spring constant was set to 15 kcal/mol/Å<sup>2</sup>, and the pulling velocity was fixed at 10 Å/ns. The nanotube and the other AA chain in the dimer were constrained to their equilibrium geometry in the two molecular assemblies. The free-energy profiles delineating the pulling processes were determined on the basis of the Jarzynski equality<sup>44</sup> over 10 independent 3 ns SMD runs, as reported in Figure 7. The free-energy barrier arising from pulling AA out of AA and Ca<sup>2+</sup>

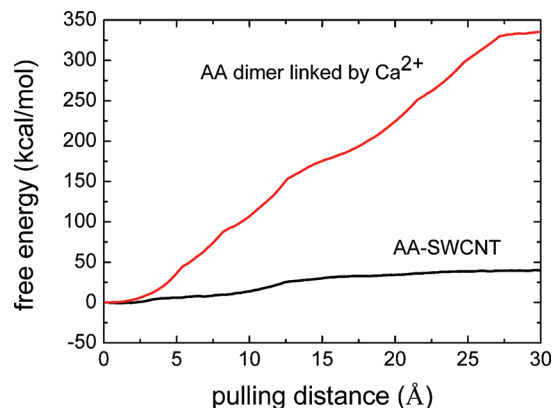


**Figure 7.** Free-energy profiles as a function of the pulling distance calculated from 10 pulling trajectories generated by combining SMD simulations with the Jarzynski identity.

appears to be much higher than that involved in the pulling of AA out of the nanotube. This result suggests that the binding affinity of AA toward AA in a Ca<sup>2+</sup>-linked dimer is much stronger than that of AA in an AA–SWCNT complex.

The stability of the AA dimer linked by Ca<sup>2+</sup> ions in the vicinity of nanotubes was also probed by simulating the molecular system consisting of the dimer and SWCNT. The starting structure of the dimer was obtained from the previous set of simulations, as shown in Figure 6a. One chain was restrained, and the nanotube was frozen and placed near the other chain. The results of the simulation indicate that Ca<sup>2+</sup> ions can link closely two chains even in the presence of the nanotube. Combining the free-energy profiles shown in Figure 7, it may, therefore, be hypothesized that, upon addition to the solution of the divalent cations, the high binding affinity of the latter toward the AA chains leads to unwrapping of AA from the nanotube, whereas the monovalent Na<sup>+</sup> cations have no effect on the AA–SWCNT-containing solution. Details of this result as well as the SMD calculations can be found in the Supporting Information.

#### 4. Conclusions

A series of atomistic MD simulations have been conducted to explore the self-assembly and the structural properties of AA–SWCNT systems, both in vacuo and in explicit water. The two representative wrapping modes, viz., compact and loose modes, that appeared in the simulations were analyzed. In the gas phase, spontaneous wrapping of the AA chain around the SWCNT resulting in a compact helical conformation is driven by van der Waals attractive and hydrogen-bonding interactions. The latter play a role of paramount importance in the formation of the compact helical structure, which is energetically favored compared to the looser helical motif. The diameter of the nanotube affects the compactness of the AA–SWCNT complexes. Formation of a perfect helical structure for an AA chain interacting with a narrow SWCNT appears to be challenging due to increasing strain. In the aqueous solution, however, the alginate chain with the carboxylate groups cannot aggregate tightly around the nanotubes on account of electrostatic repulsions and the weakening of hydrogen-bonding interactions. A loose helical wrapping mode is found to be favored. Further exploration of the free-energy landscape is, however, still necessary to confirm whether or not this mode corresponds to a global minimum. Recent successful application of REMD simulations<sup>20,21</sup> to the exploration of complexes formed by DNA and CNT provides a reasonable framework to address this issue.

The surface coverage of the nanotubes is much lower than that in the case of a compact helix, as was observed for amylose wrapping around SWCNT. AA, therefore, has the potency to dissolve more CNTs compared to amylose due to the looser wrapping mode. In addition, analysis of the MD trajectories suggests that, in GGMM sequences, the carboxylate group of every other residue prefers to face the water environment instead of the tubular surface, thereby enhancing hydrophobic interactions. Although this orientation mode is slightly different from that reported by Liu et al., a “Great Wall of China”-like motif is still observed.

Comparative investigation suggests that divalent  $\text{Ca}^{2+}$  cations can zip two AA chains together through binding to four carboxylate oxygens borne by two distinct chains, whereas monovalent  $\text{Na}^+$  cations cannot. The structure of the dimer formed is very stable, even in the presence of nanotubes. This may explain why addition of  $\text{Ca}^{2+}$  to AA–SWCNT-containing aqueous solutions results in disruption of the latter complexes. Considering the time and size scales covered by the process of spontaneous unwrapping of AA from a well wrapped AA–SWCNT system, atomistic simulation of the complete sequence of events still constitutes a daunting task and a challenging computational endeavor.

**Acknowledgment.** We would like to thank Professor Yu Liu for helpful experimental support. We are grateful to Peter Reichart for granting us the permission to use the photograph of the Great Wall of China taken in July 2008 by his late son, Thomas Reichart. This study was supported by National Natural Science Foundation of China (Nos. 20873066 and 20835002). C.C. acknowledges the French Embassy in Beijing for travel support.

**Supporting Information Available:** Additional detail on the computational methods and the simulations. Energy comparison of compact versus loose wrapping modes in vacuo. Simulation details of the amylose–SWCNT system. Energy profiles of two AA chains with  $\text{Ca}^{2+}$  ions versus with  $\text{Na}^+$  ions. Results of competitive binding of AA and SWCNT with  $\text{Ca}^{2+}$ . This material is available free of charge via the Internet at <http://pubs.acs.org>.

## References and Notes

- (1) Tasis, D.; Tagmatarchis, N.; Bianco, A.; Prato, M. *Chem. Rev.* **2006**, *106* (3), 1105–1136.
- (2) Collins, P. G.; Zettl, A.; Bando, H.; Thess, A.; Smalley, R. E. *Science* **1997**, *278* (5335), 100–103.
- (3) Liu, C.; Fan, Y. Y.; Liu, M.; Cong, H. T.; Cheng, H. M.; Dresselhaus, M. S. *Science* **1999**, *286* (5442), 1127–1129.
- (4) Sazonova, V.; Yaish, Y.; Ustunel, H.; Roundy, D.; Arias, T. A.; McEuen, P. L. *Nature* **2004**, *431* (7006), 284–287.
- (5) Portney, N. G.; Ozkan, M. *Anal. Bioanal. Chem.* **2006**, *384* (3), 620–630.
- (6) Banerjee, S.; Hemraj-Benny, T.; Wong, S. S. *Adv. Mater.* **2005**, *17* (1), 17–29.
- (7) Britz, D. A.; Khllobystov, A. N. *Chem. Soc. Rev.* **2006**, *35* (7), 637–659.
- (8) Lu, F. S.; Gu, L. R.; Mezziani, M. J.; Wang, X.; Luo, P. G.; Veca, L. M.; Cao, L.; Sun, Y. P. *Adv. Mater.* **2009**, *21* (2), 139–152.
- (9) Star, A.; Steuerman, D. W.; Heath, J. R.; Stoddart, J. F. *Angew. Chem., Int. Ed.* **2002**, *41* (14), 2508–2512.
- (10) Kim, O. K.; Je, J. T.; Baldwin, J. W.; Kooi, S.; Pehrsson, P. E.; Buckley, L. J. *J. Am. Chem. Soc.* **2003**, *125* (15), 4426–4427.
- (11) Chen, J.; Dyer, M. J.; Yu, M. F. *J. Am. Chem. Soc.* **2001**, *123* (25), 6201–6202.
- (12) Chambers, G.; Carroll, C.; Farrell, G. F.; Dalton, A. B.; McNamara, M.; Panhuis, M. I. H.; Byrne, H. J. *Nano Lett.* **2003**, *3* (6), 843–846.
- (13) Dodziuk, H.; Ejchart, A.; Anczewski, W.; Ueda, H.; Krinichnaya, E.; Dolgonos, G.; Kutner, W. *Chem. Commun.* **2003**, (8), 986–987.
- (14) Dieckmann, G. R.; Dalton, A. B.; Johnson, P. A.; Razal, J.; Chen, J.; Giordano, G. M.; Munoz, E.; Musselman, I. H.; Baughman, R. H.; Draper, R. K. *J. Am. Chem. Soc.* **2003**, *125* (7), 1770–1777.
- (15) Karajanagi, S. S.; Yang, H. C.; Asuri, P.; Sellitto, E.; Dordick, J. S.; Kane, R. S. *Langmuir* **2006**, *22* (4), 1392–1395.
- (16) Zheng, M.; Jagota, A.; Semke, E. D.; Diner, B. A.; McLean, R. S.; Lustig, S. R.; Richardson, R. E.; Tassi, N. G. *Nat. Mater.* **2003**, *2* (5), 338–342.
- (17) Tu, X. M.; Manohar, S.; Jagota, A.; Zheng, M. *Nature* **2009**, *460* (7252), 205–253.
- (18) Gao, H. J.; Kong, Y.; Cui, D. X.; Ozkan, C. S. *Nano Lett.* **2003**, *3* (4), 471–473.
- (19) Johnson, R. R.; Johnson, A. T. C.; Klein, M. L. *Nano Lett.* **2008**, *8* (1), 69–75.
- (20) Martin, W.; Zhu, W. S.; Krilov, G. *J. Phys. Chem. B* **2008**, *112* (50), 16076–16089.
- (21) Johnson, R. R.; Kohlmeyer, A.; Johnson, A. T. C.; Klein, M. L. *Nano Lett.* **2009**, *9* (2), 537–541.
- (22) Yarotski, D. A.; Kilina, S. V.; Talin, A. A.; Tretiak, S.; Prezhdo, O. V.; Balatsky, A. V.; Taylor, A. J. *Nano Lett.* **2009**, *9* (1), 12–17.
- (23) Ito, T.; Sun, L.; Crooks, R. M. *Chem. Commun.* **2003**, (13), 1482–1483.
- (24) Xie, Y. H.; Soh, A. K. *Mater. Lett.* **2005**, *59* (8–9), 971–975.
- (25) Kang, Y. K.; Lee, O.-S.; Deria, P.; Kim, S. H.; Park, T.-H.; Bonnell, D. A.; Saven, J. G.; Therien, M. J. *Nano Lett.* **2009**, *9* (4), 1414–1418.
- (26) Liu, Y.; Liang, P.; Zhang, H. Y.; Guo, D. S. *Small* **2006**, *2* (7), 874–878.
- (27) Tonnesen, H. H.; Karlsen, J. *Drug Dev. Ind. Pharm.* **2002**, *28* (6), 621–630.
- (28) Zheng, Q. B.; Xue, Q. Z.; Yan, K. O.; Hao, L. Z.; Li, Q.; Gao, X. L. *J. Phys. Chem. C* **2007**, *111* (12), 4628–4635.
- (29) Phillips, J. C.; Braun, R.; Wang, W.; Gumbart, J.; Tajkhorshid, E.; Villa, E.; Chipot, C.; Skeel, R. D.; Kale, L.; Schulten, K. *J. Comput. Chem.* **2005**, *26* (16), 1781–1802.
- (30) Kuttel, M.; Brady, J. W.; Naidoo, K. J. *J. Comput. Chem.* **2002**, *23* (13), 1236–1243.
- (31) Jorgensen, W. L.; Chandrasekhar, J.; Madura, J. D.; Impey, R. W.; Klein, M. L. *J. Chem. Phys.* **1983**, *79* (2), 926–935.
- (32) Feller, S. E.; Zhang, Y. H.; Pastor, R. W.; Brooks, B. R. *J. Chem. Phys.* **1995**, *103* (11), 4613–4621.
- (33) Darden, T.; York, D.; Pedersen, L. *J. Chem. Phys.* **1993**, *98* (12), 10089–10092.
- (34) Allen, M. P.; Tildesley, D. J. *Computer Simulation of Liquids*; Clarendon: Oxford, U.K., 1987.
- (35) Ryckaert, J. P.; Ciccotti, G.; Berendsen, H. J. C. *J. Comput. Phys.* **1977**, *23* (3), 327–341.
- (36) Andersen, H. C. *J. Comput. Phys.* **1983**, *52* (1), 24–34.
- (37) Humphrey, W.; Dalke, A.; Schulten, K. *J. Mol. Graphics.* **1996**, *14* (1), 33–38.
- (38) Grant, G. T.; Morris, E. R.; Rees, D. A.; Smith, P. J. C.; Thom, D. *FEBS Lett.* **1973**, *32* (1), 195–198.
- (39) Braccini, I.; Grasso, R. P.; Pérez, S. *Carbohydr. Res.* **1999**, *317* (1–4), 119–130.
- (40) Braccini, I.; Pérez, S. *Biomacromolecules* **2001**, *2* (4), 1089–1096.
- (41) Perry, T. D.; Cygan, R. T.; Mitchell, R. *Geochim. Cosmochim. Acta* **2006**, *70* (14), 3508–3532.
- (42) Sikorski, P.; Mo, F.; Skjåk-Bræk, G.; Stokke, B. T. *Biomacromolecules* **2007**, *8* (7), 2098–2103.
- (43) Donati, I.; Holtan, S.; Mørch, Y. A.; Borgogna, M.; Dentini, M.; Skjåk-Bræk, G. *Biomacromolecules* **2005**, *6* (2), 1031–1040.
- (44) Park, S.; Khalili-Araghi, F.; Tajkhorshid, E.; Schulten, K. *J. Chem. Phys.* **2003**, *119* (6), 3559–3566.